

HYDRA: Hybrid Robot Actions for Imitation Learning

Anonymous Author(s)

Affiliation

Address

email

1 **Abstract:** Imitation Learning (IL) is a sample efficient paradigm for robot learn-
2 ing using expert demonstrations. However, policies learned through IL suffer from
3 state distribution shift at test time, due to compounding errors in action prediction
4 which lead to previously unseen states. Choosing an action representation for
5 the policy that minimizes this distribution shift is critical in imitation learning.
6 Prior work propose using temporal action abstractions to reduce compounding
7 errors, but they often sacrifice policy dexterity or require domain-specific knowl-
8 edge. To address these trade-offs, we introduce HYDRA, a method that leverages
9 a hybrid action space with two levels of action abstractions: *sparse high-level*
10 *waypoints* and *dense low-level actions*. HYDRA dynamically switches between
11 action abstractions at test time to enable both coarse and fine-grained control of
12 a robot. In addition, HYDRA employs action relabeling to increase the consis-
13 tency of actions in the dataset, further reducing distribution shift. HYDRA
14 outperforms prior imitation learning methods by 30-40% on seven challenging
15 simulation and real world environments, involving long-horizon tasks in the real
16 world like making coffee and toasting bread. Videos are found on our website:
17 <https://tinyurl.com/3mc6793z>

18 1 Introduction

19 In recent years, supervised learning methods have made remarkable advancements in computer vi-
20 sion (CV), natural language processing (NLP), and human-level game playing [1, 2, 3, 4, 5, 6, 7].
21 In robotics, *imitation learning* (IL) has emerged as a data-driven and sample efficient approach for
22 programming robots using expert demonstrations. More specifically, behavioral cloning (BC) meth-
23 ods treat IL as a supervised learning problem and directly train a policy to map states to actions. BC
24 methods are often favored in practice for their simplicity but suffer from the well-known distribu-
25 tion shift problem, where the test time state distribution deviates from the training state distribution,
26 primarily caused by the accumulation of errors in action predictions [8, 9, 10].

27 Broadly, prior work has explored reducing distribution shift by interactively adding new data [9],
28 incorporating large prior datasets [11, 12], choosing better state representations (inputs) [13, 14],
29 or altering model or loss structure [15, 16, 14]. A less explored but critical factor is the *action*
30 representation (outputs): action prediction error partially stems from how difficult it is for the policy
31 to capture the expert demonstrated actions, so action representations are a critical line of defense
32 against distribution shift. Prior work studying action representations generally fall into two camps:
33 (1) methods that use *temporal abstractions* to treat long action sequences as a single action (i.e.,
34 reducing the effective task horizon) and thus reduce the potential for compounding errors, and (2)
35 methods that make the action representation more *expressive* to minimize the single-step prediction
36 error [17, 18, 16, 19, 15]. However, both approaches come with a number of shortcomings.

37 Methods using *temporal abstractions* often come at the cost of either the dexterity of the robot
38 or the generality to new settings. One prior approach is for the robot to follow waypoints that
39 cover multiple time steps [17, 14]; however, waypoints alone are not reactive enough for dynamic,
40 dexterous action sequences (e.g., inserting a coffee pod). Other works use structured movement

41 primitives that can capture more dynamic behaviors like skewering food items or helping a person
42 get dressed [20, 18, 21], but relying on pre-defined primitives often sacrifice generalizability to new
43 settings (e.g., new primitives beyond skewering for food manipulation). Today, we lack temporal
44 abstractions that reduce distribution shift without losing policy dexterity and generality.

45 Other methods design each action to be more *expressive* to capture the multi-modality present in
46 human behavior [19, 15, 16]; however, these expressive action spaces often lead to overfitting, high
47 training time, or complex learning objectives. Rather than making the policy more expressive, a
48 more robust approach is to make the actions in the dataset more *consistent* at a given state and easier
49 to learn (e.g., showing one consistent way to insert a coffee pod rather than many conflicting ways).
50 Prior work shows that more action consistency (e.g., consistent human demonstrators) with sufficient
51 state coverage lead to better policies [19, 14, 22], likely by reducing online policy errors [23].

52 To enable both a better temporal abstraction and more consistent actions in the dataset, our key
53 insight is to leverage the fact that most robotics tasks are hierarchical in nature – they can be divided
54 into two distinct *modes* of behaviors: *reaching high-level waypoints* (e.g., free-space motion) or
55 *fine-grained manipulation* (e.g., object interaction). Then, we can learn a policy that dynamically
56 switches between these modes – this is in fact similar to models of human decision making, where
57 it is widely believed that humans can discover action abstractions and switch between them during
58 a task [24, 25]. Capturing both waypoints and fine-grained actions enables us to compress action
59 sequences (i.e., reduce distribution shift) without sacrificing the dynamic parts of the task, thus
60 maintaining dexterity. In practice, this abstraction is general enough to represent most tasks in
61 robot manipulation. Another notable advantage of partitioning tasks into two modes is that, during
62 the waypoint reaching phase, we can *relabel* our actions with more consistent waypoint-following
63 behaviors, thus increasing action consistency in the dataset.

64 Leveraging this insight, we propose HYDRA, a method that dynamically switches between two ac-
65 tion representations: *sparse* waypoint actions for free-space linear motions and *dense*, single-step
66 delta actions for contact-rich manipulation. HYDRA learns to switch between these action modes
67 with human-labeled modes, which are provided after or during data collection with minimal ad-
68 ditional effort. In addition, HYDRA *relabels* low-level actions in the dataset during the waypoint
69 periods – where the robot is moving in free space (e.g., when reaching a coffee pod) to follow consis-
70 tent paths. These consistent actions simplify policy learning, which reduces action prediction error
71 in the dataset overall and thus reduces distribution shift. HYDRA outperforms baseline imitation
72 learning approaches across seven challenging, long-horizon manipulation tasks spanning both sim-
73 ulation and the real world. In addition, it is able to perform a complex coffee making task involving
74 many high precision stages with 80% success, 4x the performance of the best baseline, BC-RNN.

75 2 Related Work

76 **Data Curation:** Several prior works aim to *curate* data based on some notion of data quality, in
77 order to reduce distribution shift. Most works define quality as the state diversity present in a dataset,
78 To increase state diversity, Ross et al. [9] proposed to interactively collect *on-policy* demonstration
79 data, but this requires experts to label actions for newly visited states. To reduce expert supervision,
80 some methods use interventions to relabel on-policy data, where interventions can be automatically
81 or human generated [26, 27, 28, 29, 22, 30]. Laskey et al. [31] inject noise during data collection
82 to increase state diversity to achieve similar performance as interactive methods. Recent work has
83 sought to formalize a broader notion of data quality beyond just state diversity [23]. HYDRA takes
84 this broader definition into account, increasing data quality through action consistency.

85 **Model and State Priors:** Rather than changing the data, many prior works build in structure to the
86 model itself to address distribution shift. Object-centric state representations have been shown to
87 make policies more generalizable [13]. Similarly, pretrained state representations trained on multi-
88 task data have been shown to improve sample efficiency and robustness [12, 32]. Adding structure
89 into the model itself, for example using implicit representations or diffusion-based policies, has also
90 been shown to improve performance [16, 15]. The changes in HYDRA affect the action space and
91 thus are compatible with many of these prior approaches.

92 **Action Representations:** Another approach is to change the action representation to reduce com-
 93 pounding errors. One category of prior works leverage *temporal action abstractions* to reduce the
 94 number of policy steps. Several works have learned skills from demonstrations, usually requiring
 95 lots of data but struggling to generalize [33, 34, 14]. Others use parameterized action primitives
 96 or motion primitives, but despite being more sample efficient, these often require privileged state
 97 information or are not general enough for all scenes [20, 18, 21]. Waypoint action spaces have also
 98 been shown to be a sample efficient temporal abstraction; however, they fail to capture dynamic and
 99 dexterous tasks in the environment [35, 16]. For more dexterity, Johns [36] proposes Coarse-to-Fine
 100 Imitation Learning by modeling a single demonstrated trajectory as two parts: an approaching trajec-
 101 tory followed by an interaction trajectory. This approach, however, cannot easily scale to multi-step
 102 manipulation tasks with multiple stages of unstructured object interaction. HYDRA builds on these
 103 works, combining waypoints and low-level actions into one model to reduce compounding errors
 104 without losing dexterity or generality. Another category of works seek to increase the *expressiv-*
 105 *ity* of a single action to reduce action prediction error, for example with Gaussian mixture models
 106 or energy models [19, 15, 16]. However, increasing expressivity often leads to overfitting, more
 107 complex learning objectives, and increased training and evaluation time. Instead of increasing ex-
 108 pressivity, HYDRA takes a more robust approach by increasing action *consistency* in the data. Prior
 109 work shows the importance of consistent actions for minimizing distribution shift [19, 23]. HYDRA
 110 relabels actions in the dataset after data collection to increase consistency.

111 3 Preliminaries

112 Imitation learning (IL) assumes access to a dataset $\mathcal{D} = \{\tau_1, \dots, \tau_n\}$ of n expert demonstra-
 113 tions. Each demonstration τ_i is a sequence of observation-action pairs of length N_i , $\tau_i =$
 114 $\{(o_1, a_1), \dots, (o_{N_i}, a_{N_i})\}$, with observations $o \in \mathcal{O}$ and actions $a \in \mathcal{A}$. \mathcal{O} often consists of robot
 115 proprioceptive data such as end effector poses and gripper widths, denoted $s_p \in \mathcal{P}$, as well as envi-
 116 ronment observations such as images or object poses, denoted $s_e \in \mathcal{E}$, such that $\mathcal{O} = \mathcal{P} \oplus \mathcal{E}$. The
 117 true state of the environment is $s \in \mathcal{S}$. In robotics, the action space usually consists of either torque,
 118 velocity, or position commands for the robot. While velocity actions are most common, prior works
 119 also use position actions in the form of target waypoints [14, 35]. The IL objective is to learn a
 120 policy $\pi_\theta : \mathcal{O} \rightarrow \mathcal{A}$ mapping from observations to actions via the supervised loss:

$$\mathcal{L}(\theta) = -\mathbb{E}_{(o,a) \sim \mathcal{P}_{\mathcal{D}}} [\log \pi_\theta(a|o)] \quad (1)$$

121 At test time, the learned policy π_θ is rolled out under environment dynamics $f : \mathcal{S} \times \mathcal{A} \rightarrow \mathcal{S}$. Per
 122 step, we observe o_t , sample an action $\tilde{a}_t \sim \pi(\cdot|o_t)$, and obtain the next state $s_{t+1} = f(s_t, \tilde{a}_t)$.

123 **Distribution Shift in IL.** A fundamental challenge with imitation learning is state *distribution shift*
 124 between training and test time. Considering training sample $(\dots, o_t, a_t, o_{t+1} \dots)$: if the learned
 125 policy outputs $\tilde{a}_t \sim \pi(\cdot|o_t)$, which has a small action error $\epsilon_t = \tilde{a}_t - a_t$, the next state following
 126 this action will also deviate: $\tilde{s}_{t+1} = f(s_t, a_t + \epsilon_t)$, which in turn affects the policy output at the
 127 next step. For real world dynamics, this change in next state can be highly disproportionate to $\|\epsilon_t\|$.
 128 For example in the coffee task in Fig. 1, with a slight change in gripper position (small ϵ_t) the policy
 129 can misgrasp the coffee pod (large change in s_{t+1} and o_{t+1}). Furthermore, noise in the dynamics
 130 f can lead to even larger changes in o_{t+1} . As we continue to execute for the next $N - t$ steps, this
 131 divergence from the training distribution can compound, often leading to task failure.

132 Therefore, reducing distribution shift requires reducing ϵ_t for all $t \in \{1, \dots, N\}$ or increasing the
 133 coverage of states s_t . One approach to reduce policy error is increasing **action consistency**, which
 134 prior work defines as lowering the entropy of the expert policy π_E at each state: $\mathcal{H}_{\pi_E}(a|s)$ [23].
 135 However, there is a trade-off between state coverage and action consistency during data collection,
 136 since less consistent actions often lead to more diverse states [23, 19]. HYDRA reduces distribution
 137 shift by using a temporal abstraction for the action space – which shortens the number of policy
 138 steps N and thus reduces compounding errors – and by improving action consistency in offline data
 139 – which reduces $\|\epsilon_t\|$ without reducing state coverage.

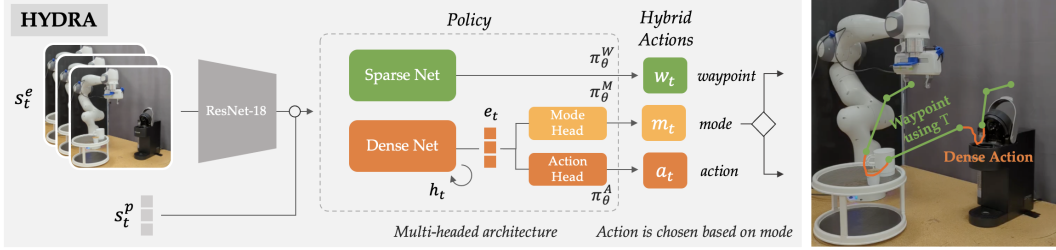


Figure 1: Multi-headed architecture of HYDRA: During training, we learn to predict waypoints, low level actions, and the mode label for each time step. One network (Dense Net) predicts the low level action a_t and the mode m_t ; both the action and mode heads of Dense Net share an intermediate representation e_t . A separate network (Sparse Net) predicts the high level waypoint w_t . At test time, we sample m_t and either servo to reach a waypoint ($m_t = 0$) without requering the policy, or follow a dense action for one time step ($m_t = 1$). An example of how sparse and dense modes can be arbitrarily stitched together at test time is shown on the right.

140 4 HYDRA: A Hybrid Action Representation

141 To reduce distribution shift, our insight is that most robot manipulation tasks are a combination of
 142 *sparse* waypoint-reaching, such as reaching for an object or lifting a mug towards a shelf, and *dense*
 143 low-level actions, such as grasping an object or balancing a mug stably on a shelf. Waypoints capture
 144 free-space motions but struggle to capture dexterous or precise behaviors. Conversely, low-level
 145 actions capture these dynamic behaviors but are often redundant during long free-space motions.

146 Instead of learning from only velocities or waypoints, HYDRA learns a *hybrid action representation*
 147 consisting of both high-level waypoints in the robot’s proprioceptive space $w \in \mathcal{P}$ and low-level ac-
 148 tions $a \in \mathcal{A}$. Additionally, we learn to dynamically switch between these modes by predicting which
 149 mode $m \in \{0, 1\}$, sparse or dense, should be executed at each demonstrated state. Mode labels are
 150 annotated with little extra cost by experts either during or after data collection. This flexible ab-
 151 straction leads to (1) a compressed action space that reduces compounding errors without sacrificing
 152 dexterity or generality, and (2) a more consistent, simple low-level action distribution through action
 153 relabeling during the sparse periods. This section presents an overview of the approach, followed by
 154 discussions on mode labeling, action relabeling, and training/testing procedures.

155 **Overview:** The multi-headed architecture of HYDRA is outlined in Fig. 1, with heads $\pi_\theta^M : \mathcal{O} \rightarrow$
 156 $\{0, 1\}$, $\pi_\theta^A : \mathcal{O} \rightarrow \mathcal{A}$, $\pi_\theta^W : \mathcal{O} \rightarrow \mathcal{P}$, for mode, action, and waypoint respectively. One network,
 157 Dense Net, predicts the low-level action a_t and the mode m_t at each input $o_t = \{s_t^e, s_t^p\}$. Another
 158 network, Sparse Net, separately outputs the desired *future* waypoint w_t for input o_t . We assume
 159 waypoints can be reached using a known controller $T : \mathcal{O} \times \mathcal{P} \rightarrow \mathcal{A}$ which converts the state
 160 and desired waypoint into a low-level action (e.g. a linear controller, see the right side of Fig. 1). In
 161 practice, Dense Net is recurrent since both the mode and action are highly history-dependent. Sparse
 162 Net in contrast only uses the current observation, since waypoints are less multi-modal and history
 163 dependent than actions. Then at test time, HYDRA predicts the mode m_t and follows the controller
 164 T until reaching the waypoint during predicted sparse periods, and follows low-level actions at each
 165 step during predicted dense periods. See Appendix C for more details.

166 4.1 Data Processing: Mode Labeling and Action Consistency

167 To dynamically switch action abstractions, we need labeled modes m_t , waypoints w_t , and actions
 168 a_t at each time step. We first obtain binary mode labels m_t from humans, and then use the mode
 169 labels to extract waypoints and to relabel low-level actions. Importantly, modes can be labeled either
 170 online (during demonstration collection, e.g. with a simple button interface), or entirely offline (after
 171 demonstration collection, e.g., labeling each frame with its mode). With modes labeled, we can
 172 segment each demonstration into sparse waypoint and dense action phases. We provide the details
 173 of the labeling and segmentation process in Appendix B. For each sparse phase, we can extract the
 174 desired future waypoint w_t at o_t : if $m_t = 0$ (sparse), the future waypoint is final proprioceptive
 175 state $w_t = p_{t'}$ in that sparse segment, where $t' > t$. But if $m_t = 1$ (dense), the waypoint is the next
 176 proprioceptive state $w_t = p_{t+1}$. This yields a dataset of $\hat{\mathcal{D}}$ of (o, a, w, m) tuples. Now the policy
 177 has full supervision to learn the modes, waypoints, and actions.

178 **Mode Labeling Strategy:** Since waypoints will be reached online with controller T, the main
 179 requirement for labeling modes is that during sparse phases ($m_t = 0$), the labeled waypoint w_t
 180 should be reachable via T starting from o_t (i.e., without collision): for example, if the demonstrator
 181 starts in free space and labels a waypoint close to coffee K-pod, and if the policy uses a linear P-
 182 controller as T, then the K-pod waypoint should be reachable from the initial pose in a straight-line
 183 path. Otherwise, the learned policy might collide when it tries to reach similar waypoints. We do not
 184 assume access to a collision-avoidance planner as T in this work, but if one has access to a planner
 185 then T can always reach the desired waypoint, so this reachability requirement can be ignored. Other
 186 considerations for mode labeling and a discussion of mode sensitivity is provided in [Appendix B](#).
 187 We specifically show that our method is not overly sensitive to mode labeling strategies outside of
 188 the collision-free requirement above. Furthermore, we show that mode labels can be learned from
 189 substantially fewer examples without a major effect on performance [Appendix D.3](#).

190 **Relabeling Low-Level Actions:** As discussed in [Section 3](#), action consistency can improve policy
 191 performance by simplifying the BC objective in [Eq. \(1\)](#) and thus reducing $\|\epsilon_t\|$, provided the data
 192 has enough state coverage. However, making actions consistent during data collection is challenging
 193 and can often reduce state coverage [\[22\]](#), so instead HYDRA performs *offline* action relabeling, i.e.,
 194 after collection. To relabel human actions a_t during the sparse periods, HYDRA uses waypoint
 195 controller T to “imagine” a new action at each demonstrated robot state s_t^p based on the waypoint
 196 w_t . We lack a consistent relabeling strategy for dense periods, so we leave this to future work.

197 However, a subtle challenge with offline relabeling is that changing the actions in the data can put the
 198 policy out of distribution at test time, since new actions can lead to new states online. For example,
 199 if an arc path was demonstrated to get to a waypoint, but a linear controller is used for relabeling, the
 200 linear action will take us off that path. HYDRA avoids this problem by using a waypoint controller
 201 T online during sparse periods, meaning relabeled actions will not be deployed online. Rather, this
 202 action relabeling serves primarily to simplify the dense action learning objective of HYDRA and
 203 increase action consistency in the overall dataset.

204 A natural question arises: since sparse actions will be executed with T online, could we instead
 205 further simplify learning by avoiding training on dense actions during sparse periods? If HYDRA
 206 mispredicts a sparse mode as dense, then the dense actions will still be executed online, so HYDRA
 207 should still be trained on dense actions during sparse periods as a back-up. We show that reducing
 208 the training weight of dense actions during sparse periods hurts performance in [Appendix D.5](#).

209 4.2 Training and Evaluation

210 **Training:** HYDRA is trained to both imitate low-level actions a with policy π_θ^A , high-level way-
 211 points w with π_θ^W , and the mode m with π_θ^M at each time step. To balance the waypoint and action
 212 losses, we use a mode-specific loss at each time step that weighs the current mode’s loss with $(1-\gamma)$,
 213 and the other mode’s loss with γ . Given a processed dataset $\hat{\mathcal{D}}$ consisting of tuples of (o, a, w, m) ,
 214 we modify the loss in [Eq. \(1\)](#) with the new heads of HYDRA (mode, action, and waypoint):

$$\mathcal{L}_a(\theta) = -\mathbb{E}_{(o,a,w,m) \sim p_{\hat{\mathcal{D}}}} [(1 - \alpha_m) \log \pi_\theta^A(a|o) + \alpha_m \log \pi_\theta^W(w|o)] \quad (2)$$

$$\mathcal{L}_m(\theta) = -\mathbb{E}_{(o,a,w,m) \sim p_{\hat{\mathcal{D}}}} [m \log \pi_\theta^M(m = 1|o) + (1 - m) \log \pi_\theta^M(m = 0|o)] \quad (3)$$

215 \mathcal{L}_a weighs the BC loss for waypoints and actions by the current mode: $\alpha_m = m\gamma + (1 - m)(1 - \gamma)$
 216 is the mode-specific weight for the sparse waypoint part of \mathcal{L}_a . If we are in sparse mode ($m = 0$),
 217 then $\alpha_m = 1 - \gamma$, but in dense mode, $\alpha_m = \gamma$. Thus, a low gamma encourages the model to fit the
 218 loss for the current mode *more* than the loss for the other mode, and $\gamma = 0.5$ will be a mode-agnostic
 219 weighting. See [Appendix D.5](#) for results of ablating γ . \mathcal{L}_m is the mode cross entropy classification
 220 loss. Combining these terms with mode loss weight β , we get the full HYDRA objective:

$$\mathcal{L}(\theta) = \mathcal{L}_a(\theta) + \beta \mathcal{L}_m(\theta) \quad (4)$$

221 **Evaluation:** During evaluation, the policy chooses the mode using \tilde{m}_t . If $\tilde{m}_t = 0$, the model will
 222 servo in a closed-loop fashion to the predicted waypoint \tilde{w}_t using controller T. The policy is queried
 223 at every step to continually update the policy hidden state, but importantly its outputs are ignored
 224 until we reach the waypoint to avoid action prediction errors. If $\tilde{m}_t = 1$, the model will execute just
 225 the next step using the predicted dense action \tilde{a}_t .

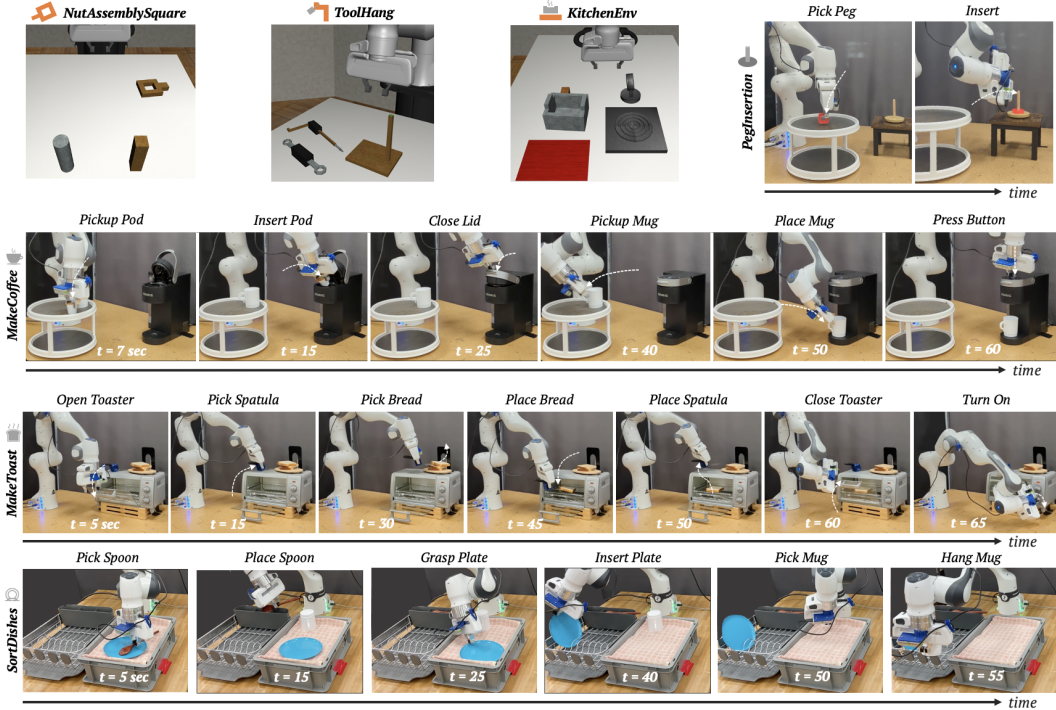


Figure 2: Simulation & Real-world environments, with task stages shown for real world tasks. **Simulation:** In *NutAssemblySquare*, the task is to pick up a square nut at various positions and orientations and insert it onto a vertical square peg. In *ToolHang*, a hanging frame is inserted onto a fixed stand, followed by placing a tool on the frame. Both the frame and tool poses are randomized. Frame insertion is challenging due to the small insertion area. *KitchenEnv* involves turning on a stove, moving a pot onto the stove, putting an object in the pot, then moving the pot to a serving area. **Real World:** *PegInsertion* involves inserting a peg with a hole in the center onto a round insertion rod (top right); the peg location and geometry are varied. *MakeCoffee* is a 6-step task (top middle row) involving picking up a K-pod, inserting it into a Keurig machine, closing the lid of the Keurig, positioning a mug, and then pressing start on the Keurig; the K-pod location and mug orientations are varied. This is a more challenging version of the task used in prior work [13], which did not include the mug component. *MakeToast* has 7-steps (bottom middle row): a hinged toaster oven is opened, a spatula is picked up, bread is placed inside the toaster, the toaster is closed, and the timer dial is turned to start. Both bread and spatula initial poses vary. *SortDishes* (bottom row) has 6 stages: pick up spoon, place spoon in rack, grasp plate and insert it into rack, and grasp mug and hang the mug. All objects vary in initial pose.

226 5 Experiments

227 We evaluate the performance of HYDRA in 3 challenging simulation environments and 4 complex
 228 real world tasks, shown in Fig. 2. These tasks cover a wide range of affordances and levels of
 229 precision, from precisely inserting a coffee pod to picking up bread with a spatula. See Appendix C
 230 for model hyperparameters, data collection, and training details. Videos can be found on our website.

231 **Data Collection:** We leverage proficient human demonstration data for simulated tasks from
 232 robomimic [19]. Mode labels and waypoints were annotated offline for simulation datasets as de-
 233 scribed in Appendix B. Demonstrations for real world tasks were collected by a proficient user using
 234 VR teleoperation using an Oculus Quest 2. Mode labels and waypoints were provided during data
 235 collection (online) using the side button on the Quest VR controller with no added collection time.

236 **Simulation:** In Fig. 3 (top row), we compare our method to BC and BC-RNN for the *NutAssem-*
 237 *blySquare* and *ToolHang* tasks (state-based), as well as the *KitchenEnv* task (vision-based) from
 238 robosuite (see top row in Fig. 2). Our method improves performance on the *NutAssemblySquare*
 239 task, where baselines are already quite strong. We also ablate the data size from 200 demos to 100
 240 and 50 in Fig. 3, illustrating that HYDRA is more sample efficient than baselines, with the gap grow-
 241 ing as data size decreases. HYDRA-NR in Fig. 3 removes action relabeling and drops performance
 242 by 8%, which we attribute to high action multi-modality in non-relabeled sparse periods.

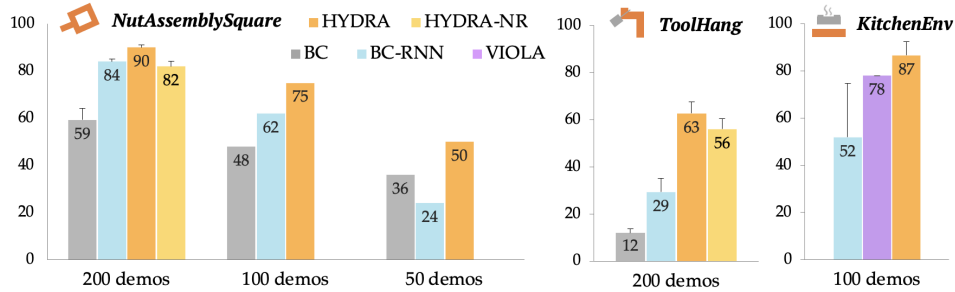


Figure 3: Sim Results for HYDRA vs. BC, BC-RNN, and VIOLA: best checkpoint success rate averaged over three seeds. **Left to Right:** *NutAssemblySquare* (state), *ToolHang* (state), and *KitchenEnv* (vision) tasks. HYDRA beats baselines on all of these tasks, and even beats VIOLA [13] on the kitchen task despite using a much smaller and simpler model. We also show a comparison for BC-RNN and HYDRA with decreasing data sizes for *NutAssemblySquare*, showing that our method is more sample efficient than BC-RNN. HYDRA without action relabeling (HYDRA-NR, *NutAssemblySquare* and *ToolHang*) drops performance by 7-8%.

243 For the *Tool Hang* task (top middle in Fig. 3), which is long horizon and consists of many waypoint
 244 and dense periods and requiring much higher precision, our method has an even bigger gap in per-
 245 formance with BC and BC-RNN. While the best baseline gets 29%, our method reaches 63% with
 246 the same inputs. Once again, removing action relabeling (HYDRA-NR) drops performance by 7%
 247 but is still substantially better than baseline.

248 For *KitchenEnv* (vision-based), we also compare to VIOLA [13], an image-based model that uses
 249 bounding box features and a large transformer architecture to predict actions. Once again, HYDRA
 250 is able to outperform BC-RNN by 35% on this long horizon task. HYDRA also outperforms VIOLA
 251 by 9%, despite using a simpler and smaller model.

252 In Appendix D, we show a waypoint-only baseline, mode labeling strategy ablations, and a
 253 relabeling-only ablation where action consistency is improved but the waypoint controller is not
 254 used online. In Appendix D.3, we show that mode labels can be learned with fewer examples with-
 255 out a large drop in performance (e.g., using 25% of mode labels drops performance by 10%).

256 **Real World:** In Fig. 4, we compare our method to BC-RNN (vision-based) for four high precision
 257 tasks: *PegInsertion*, *MakeCoffee*, *MakeToast*, and *SortDishes*. The latter three are long-horizon, and
 258 Fig. 4 shows cumulative success per task stage. In *PegInsertion*, our method substantially outper-
 259 forms BC-RNN at both peg grasping and precise insertion portions of the task, thanks to combining
 260 precise waypoints with flexible low level actions where necessary.

261 For *MakeCoffee*, HYDRA once again beats BC-RNN and VIOLA by a substantial margin at all
 262 stages of the task. Although all methods perform well in grasping the K-pod, the performance of
 263 the baselines declines rapidly in the following phases. While BC-RNN failed to do this task in prior
 264 work, we see that with a bit of parameter tuning, BC-RNN is a strong baseline, achieving 20%
 265 performance [13]. The reported performance of VIOLA in prior work for coffee pod insertion and
 266 closing the lid is 60%, which matches with the performance we observe for the corresponding stage
 267 of our coffee task. Our task adds two more stages (picking up and placing a mug before pressing the
 268 button), interestingly causing the final success rate of VIOLA to drop to 20%, the same as BC-RNN.
 269 Using the same parameters and model size as BC-RNN, HYDRA achieves 80% final success at this
 270 task with the same underlying dataset.

271 For *MakeToast* and *SortDishes*, HYDRA performs better on all stages of the task as compared to
 272 BC-RNN. We omit VIOLA in these tasks since, as seen in the coffee task, BC-RNN is a competitive
 273 baseline. Both tasks consists of several bottleneck stages where performance drops sharply. In
 274 *MakeToast*, for picking up bread, the spatula must slide underneath a bread slice – HYDRA passes
 275 this stage 70% of the time, beating BC-RNN by 30%. The last stage (turning the toaster on) is
 276 particularly challenging for all methods, but HYDRA completes it 20% of the time compared to
 277 0% for BC-RNN. In *SortDishes*, the final hang-mug stage similarly requires high precision with
 278 randomized objects. Not including the challenging last stage, HYDRA beats BC-RNN by 40% on
 279 this task. See Appendix D.1 for rollouts of each task for each model.

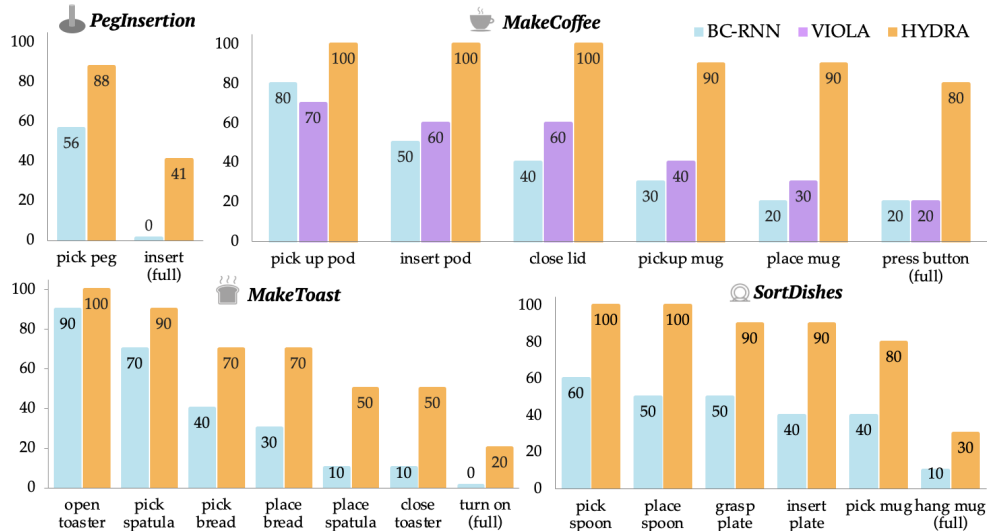


Figure 4: Real Results for HYDRA vs. BC, BC-RNN, and VIOLA. The x-axis denotes each stage (right-most value is the final success rate). **Top Left:** HYDRA vs. BC-RNN on the real *PegInsertion* task for 50 demos under 32 rollouts across 4 different nuts. This task requires very precise grasping and insertion of multiple types of nuts, which our method does with high success. While baseline is unable to perform insertion, HYDRA gets 41% success. **Top Right:** *MakeCoffee* long-horizon task for 100 demos under 10 rollouts. Our method beats baseline by 60%. **Bottom Left:** *MakeToast* long-horizon task for 100 demos under 10 rollouts. While both methods struggle to turn the toaster on, HYDRA is able to reach 50% success for 6/7 stages compared to 10% for baseline. **Bottom Right:** *SortDishes* for 100 demos under 10 rollouts. Waypoints in HYDRA precisely capture the diverse poses in this task, beating BC-RNN by 40% and 20% for the last two stages.

280 We observe that the performance gain for HYDRA in our real world experiments is notably higher
 281 than in simulation. We hypothesize this is due to (1) higher variance in action playback on the
 282 real robot setup, which HYDRA mitigates during sparse periods using the closed-loop waypoint
 283 controller, and (2) increased potential for compounding errors in longer tasks. Overall, HYDRA is
 284 well-suited to long horizon tasks even with many high-precision bottleneck stages, due to its ability
 285 to switch between waypoints and dense actions and its ability to increase action consistency offline.
 286 We also observed that in our real world tasks, HYDRA exhibits emergent retrying behavior, often
 287 re-servoing to a consistent and in-distribution waypoint to retry a failed dense period.

288 6 Discussion

289 **Summary:** In this work, we propose HYDRA, which uses a flexible action abstraction to reduce
 290 compounding errors, and improves action consistency while maintaining the state diversity present
 291 in uncurated human demonstrations. HYDRA learns to dynamically switch between following way-
 292 points and taking low level actions with a small amount of added mode label supervision that can be
 293 provided either online or offline. HYDRA substantially outperforms baselines on three simulation
 294 tasks and four real world tasks that involve long horizon manipulation with many bottleneck states.

295 **Limitations & Future Work:** While only a minor amount of added supervision, HYDRA relies on
 296 having expert-collected mode labels. We show that mode labels can be learned from much less data
 297 in [Appendix D.3](#), but future work might consider using unsupervised methods for mode labeling,
 298 e.g., skill segmentation [37] or automatically extracting “linear” portions of a demonstration. We
 299 also hypothesize multi-task datasets can help learn a general mode-predictor that can be fine-tuned
 300 or deployed zero-shot on novel tasks. Furthermore, when mode labels are collected online, mode
 301 labeling can add a mental load for the demonstrator and might also influence the quality of the data
 302 on its own. Future work might conduct more extensive user studies to better understand the effect
 303 of providing mode labels for both the demonstrator and the final learning performance.

304 Despite these limitations, HYDRA is a simple and easy-to-implement method, and it is exciting that
 305 it shows substantial improvement over state-of-the-art imitation learning techniques and significant
 306 promise in solving challenging manipulation tasks in the real world.

References

- 307
- 308 [1] A. Dosovitskiy, L. Beyer, A. Kolesnikov, D. Weissenborn, X. Zhai, T. Unterthiner, M. De-
309 hghani, M. Minderer, G. Heigold, S. Gelly, et al. An image is worth 16x16 words: Transform-
310 ers for image recognition at scale. In *International Conference on Learning Representations*,
311 2020.
- 312 [2] K. He, X. Chen, S. Xie, Y. Li, P. Dollár, and R. Girshick. Masked autoencoders are scalable
313 vision learners. In *Proceedings of the IEEE/CVF Conference on Computer Vision and Pattern
314 Recognition*, pages 16000–16009, 2022.
- 315 [3] A. Radford, J. W. Kim, C. Hallacy, A. Ramesh, G. Goh, S. Agarwal, G. Sastry, A. Askell,
316 P. Mishkin, J. Clark, et al. Learning transferable visual models from natural language supervi-
317 sion. In *International conference on machine learning*, pages 8748–8763. PMLR, 2021.
- 318 [4] T. Brown, B. Mann, N. Ryder, M. Subbiah, J. D. Kaplan, P. Dhariwal, A. Neelakantan,
319 P. Shyam, G. Sastry, A. Askell, et al. Language models are few-shot learners. *Advances
320 in neural information processing systems*, 33:1877–1901, 2020.
- 321 [5] R. Thoppilan, D. De Freitas, J. Hall, N. Shazeer, A. Kulshreshtha, H.-T. Cheng, A. Jin, T. Bos,
322 L. Baker, Y. Du, et al. Lamda: Language models for dialog applications. *arXiv preprint
323 arXiv:2201.08239*, 2022.
- 324 [6] A. Chowdhery, S. Narang, J. Devlin, M. Bosma, G. Mishra, A. Roberts, P. Barham, H. W.
325 Chung, C. Sutton, S. Gehrmann, et al. Palm: Scaling language modeling with pathways. *arXiv
326 preprint arXiv:2204.02311*, 2022.
- 327 [7] S. Reed, K. Zolna, E. Parisotto, S. G. Colmenarejo, A. Novikov, G. Barth-Maron, M. Gimenez,
328 Y. Sulsky, J. Kay, J. T. Springenberg, et al. A generalist agent. *arXiv preprint
329 arXiv:2205.06175*, 2022.
- 330 [8] S. Ross and D. Bagnell. Efficient reductions for imitation learning. In *Proceedings of the thir-
331 teenth international conference on artificial intelligence and statistics*, pages 661–668. JMLR
332 Workshop and Conference Proceedings, 2010.
- 333 [9] S. Ross, G. Gordon, and D. Bagnell. A reduction of imitation learning and structured predic-
334 tion to no-regret online learning. In *Proceedings of the fourteenth international conference
335 on artificial intelligence and statistics*, pages 627–635. JMLR Workshop and Conference Pro-
336 ceedings, 2011.
- 337 [10] J. Spencer, S. Choudhury, A. Venkatraman, B. Ziebart, and J. A. Bagnell. Feedback in imitation
338 learning: The three regimes of covariate shift. *arXiv preprint arXiv:2102.02872*, 2021.
- 339 [11] D. Driess, F. Xia, M. S. M. Sajjadi, C. Lynch, A. Chowdhery, B. Ichter, A. Wahid, J. Tompson,
340 Q. Vuong, T. Yu, W. Huang, Y. Chebotar, P. Sermanet, D. Duckworth, S. Levine, V. Vanhoucke,
341 K. Hausman, M. Toussaint, K. Greff, A. Zeng, I. Mordatch, and P. Florence. Palm-e: An
342 embodied multimodal language model. In *arXiv preprint arXiv:2303.03378*, 2023.
- 343 [12] S. Karamcheti, S. Nair, A. S. Chen, T. Kollar, C. Finn, D. Sadigh, and P. Liang. Language-
344 driven representation learning for robotics. 2023.
- 345 [13] Y. Zhu, A. Joshi, P. Stone, and Y. Zhu. Viola: Imitation learning for vision-based manipulation
346 with object proposal priors. *6th Annual Conference on Robot Learning (CoRL)*, 2022.
- 347 [14] S. Belkhale and D. Sadigh. Plato: Predicting latent affordances through object-centric play. In
348 *6th Annual Conference on Robot Learning*, 2022.
- 349 [15] P. Florence, C. Lynch, A. Zeng, O. A. Ramirez, A. Wahid, L. Downs, A. Wong, J. Lee, I. Mor-
350 datch, and J. Tompson. Implicit behavioral cloning. In *Conference on Robot Learning*, pages
351 158–168. PMLR, 2022.

- 352 [16] C. Chi, S. Feng, Y. Du, Z. Xu, E. Cousineau, B. Burchfiel, and S. Song. Diffusion policy:
353 Visuomotor policy learning via action diffusion. *arXiv preprint arXiv:2303.04137*, 2023.
- 354 [17] M. Shridhar, L. Manuelli, and D. Fox. Perceiver-actor: A multi-task transformer for robotic
355 manipulation. In *6th Annual Conference on Robot Learning*, 2022.
- 356 [18] R. P. Joshi, N. Koganti, and T. Shibata. A framework for robotic clothing assistance by imita-
357 tion learning. *Advanced Robotics*, 33(22):1156–1174, 2019.
- 358 [19] A. Mandlekar, D. Xu, J. Wong, S. Nasiriany, C. Wang, R. Kulkarni, L. Fei-Fei, S. Savarese,
359 Y. Zhu, and R. Martín-Martín. What matters in learning from offline human demonstrations
360 for robot manipulation. *arXiv preprint arXiv:2108.03298*, 2021.
- 361 [20] P. Sundaresan, S. Belkhale, and D. Sadigh. Learning visuo-haptic skewering strategies for
362 robot-assisted feeding. In *6th Annual Conference on Robot Learning*, 2022. URL <https://openreview.net/forum?id=1Lq09gVoaTE>.
- 364 [21] J. Silvério, Y. Huang, F. J. Abu-Dakka, L. Rozo, and D. G. Caldwell. Uncertainty-aware
365 imitation learning using kernelized movement primitives. In *2019 IEEE/RSJ International
366 Conference on Intelligent Robots and Systems (IROS)*, pages 90–97. IEEE, 2019.
- 367 [22] K. Gandhi, S. Karamcheti, M. Liao, and D. Sadigh. Eliciting compatible demonstrations for
368 multi-human imitation learning. In *Proceedings of the 6th Conference on Robot Learning
369 (CoRL)*, 2022.
- 370 [23] S. Belkhale, Y. Cui, and D. Sadigh. Data quality in imitation learning, 2023.
- 371 [24] L. L. Richmond and J. M. Zacks. Constructing experience: Event models from perception to
372 action. *Trends in Cognitive Sciences*, 21(12):962–980, 2017. ISSN 1364-6613. doi:<https://doi.org/10.1016/j.tics.2017.08.005>. URL <https://www.sciencedirect.com/science/article/pii/S1364661317301857>.
- 375 [25] C. Baldassano, J. Chen, A. Zadbood, J. Pillow, U. Hasson, and K. Norman. Discovering event
376 structure in continuous narrative perception and memory, 2016.
- 377 [26] Y. Cui, D. Isele, S. Niekum, and K. Fujimura. Uncertainty-aware data aggregation for deep
378 imitation learning. In *2019 International Conference on Robotics and Automation (ICRA)*,
379 pages 761–767. IEEE, 2019.
- 380 [27] R. Hoque, A. Balakrishna, E. Novoseller, A. Wilcox, D. S. Brown, and K. Goldberg.
381 Thriftydagger: Budget-aware novelty and risk gating for interactive imitation learning. In
382 *Conference on Robot Learning*, pages 598–608. PMLR, 2022.
- 383 [28] M. Kelly, C. Sidrane, K. Driggs-Campbell, and M. J. Kochenderfer. Hg-dagger: Interactive
384 imitation learning with human experts. In *2019 International Conference on Robotics and
385 Automation (ICRA)*, pages 8077–8083. IEEE, 2019.
- 386 [29] A. Mandlekar, D. Xu, R. Martín-Martín, Y. Zhu, L. Fei-Fei, and S. Savarese. Human-in-the-
387 loop imitation learning using remote teleoperation. *arXiv preprint arXiv:2012.06733*, 2020.
- 388 [30] M. L. Schrum, E. Hedlund-Botti, N. Moorman, and M. C. Gombolay. Mind meld: Personal-
389 ized meta-learning for robot-centric imitation learning. In *2022 17th ACM/IEEE International
390 Conference on Human-Robot Interaction (HRI)*, pages 157–165. IEEE, 2022.
- 391 [31] M. Laskey, J. Lee, R. Fox, A. Dragan, and K. Goldberg. Dart: Noise injection for robust
392 imitation learning. In *Conference on robot learning*, pages 143–156. PMLR, 2017.
- 393 [32] S. Nair, A. Rajeswaran, V. Kumar, C. Finn, and A. Gupta. R3m: A universal visual repre-
394 sentation for robot manipulation. In *6th Annual Conference on Robot Learning*, 2022. URL
395 <https://openreview.net/forum?id=tGbpz6yOrI>.

- 396 [33] K. Pertsch, Y. Lee, and J. J. Lim. Accelerating reinforcement learning with learned skill priors.
397 In *Conference on Robot Learning (CoRL)*, 2020.
- 398 [34] C. Lynch, M. Khansari, T. Xiao, V. Kumar, J. Tompson, S. Levine, and P. Sermanet. Learning
399 latent plans from play. In *Conference on robot learning*, pages 1113–1132. PMLR, 2020.
- 400 [35] M. Shridhar, L. Manuelli, and D. Fox. Perceiver-actor: A multi-task transformer for robotic
401 manipulation. In *6th Annual Conference on Robot Learning*, 2022. URL [https://openre-](https://openreview.net/forum?id=PS_eCS_WCvD)
402 [view.net/forum?id=PS_eCS_WCvD](https://openreview.net/forum?id=PS_eCS_WCvD).
- 403 [36] E. Johns. Coarse-to-fine imitation learning: Robot manipulation from a single demonstration.
404 In *2021 IEEE international conference on robotics and automation (ICRA)*, pages 4613–4619.
405 IEEE, 2021.
- 406 [37] T. Kipf, Y. Li, H. Dai, V. Zambaldi, A. Sanchez-Gonzalez, E. Grefenstette, P. Kohli, and
407 P. Battaglia. CompILE: Compositional imitation learning and execution. In K. Chaudhuri
408 and R. Salakhutdinov, editors, *Proceedings of the 36th International Conference on Ma-*
409 *chine Learning*, volume 97 of *Proceedings of Machine Learning Research*, pages 3418–3428.
410 PMLR, 09–15 Jun 2019. URL [https://proceedings.mlr.press/v97/kipf19a.](https://proceedings.mlr.press/v97/kipf19a.html)
411 [html](https://proceedings.mlr.press/v97/kipf19a.html).
- 412 [38] M. Andrychowicz, F. Wolski, A. Ray, J. Schneider, R. Fong, P. Welinder, B. McGrew, J. To-
413 bin, O. Pieter Abbeel, and W. Zaremba. Hindsight experience replay. *Advances in neural*
414 *information processing systems*, 30, 2017.
- 415 [39] L. Zhang and B. C. Stadie. Understanding hindsight goal relabeling requires rethinking diver-
416 gence minimization. In *Deep Reinforcement Learning Workshop NeurIPS 2022*.

417 We provide a broader discussion of our method in this appendix. In [Appendix A](#) we list a set of
418 *motivating* questions that may arise during reading the main text of this work and provide our re-
419 sponse with links to additional details in corresponding sections in the Appendix. In [Appendix B](#) we
420 discuss how to collect mode labels, and considerations for how to define waypoint and dense seg-
421 ments. In [Appendix C](#), we outline training procedures, model architectures, and hyperparameters.
422 In [Appendix D](#), we provide ablation experiments for our method, including sensitivity to mode la-
423 bels, learning mode labels from less data, ablations to γ , and robustness of HYDRA to added system
424 noise.

425 A Motivating Questions

426 **Intuitively, why does HYDRA help improve BC?** Humans demonstrate manipulation tasks at an
427 abstraction level that is different from how the robot interprets the data. A BC agent interprets the
428 data *literally* as taking a specific action at an exact state while the human is *noisily* reaching for an
429 object. At the high level, HYDRA improves BC by realigning the task abstraction of the robot to
430 the human demonstrator during waypoint mode of the task. Concretely, HYDRA curates the dataset
431 in a way that improves action consistency and optimality without reducing state diversity and hence
432 allowing the learned policy to stay closer in distribution at test time.

433 **What’s the relationship of HYDRA with works in hindsight relabeling?** Hindsight relabel-
434 ing [38] is the idea of relabeling past experiences of goal-reaching trajectories with the final state it
435 reaches to reuse any sub-optimal data (especially for reinforcement learning settings). Recent work
436 of Zhang and Stadie [39] draws the connection between goal-conditioned imitation learning and
437 hindsight relabeling from a divergence-minimization perspective. The current implementation of
438 HYDRA operates in single-task imitation learning setting, and therefore is only remotely related to
439 the idea in hindsight relabeling. From this perspective, one can think of HYDRA as effectively re-
440 ducing divergence of the dataset’s action distribution by relabeling actions for the waypoint periods
441 of the trajectory.

442 **Does online mode labeling change demonstrator behavior?** We explain the online mode labeling
443 process in [Appendix B](#). We acknowledge that asking the demonstrator to provide online mode label-
444 ing adds additional cognitive load during demonstrating the task, and at the same time may change
445 their demonstration behavior. In practice, asking the demonstrator to provide the two mode labels
446 can communicate the structure the robot leverages to learn tasks and may in turn allow the human
447 to provide better demonstrations (such as consistent waypoints etc.). However, we leave this user
448 study to future work.

449 **How sensitive is HYDRA to mode labeling?** In our experiments, we (experts in this task) provided
450 the mode labels for different tasks. We found HYDRA to be robust to the labeling strategies across
451 the two labelers. For simulated environments, we use existing datasets and labeled the modes using
452 an interface that shows the robot view of the task and the human annotator marks whether a frame is
453 waypoint or dense mode. For real robot tasks, the human demonstrator provides the mode labels as
454 they provide the demonstration using a button on the teleoperation controller. We provide guidelines
455 for how to perform mode labeling in [Appendix B](#).

456 B Labeling Modes in HYDRA

457 B.1 Providing Mode Labels

458 The primary assumption made in HYDRA is the availability of mode labels for sparse and dense
459 periods. Here we provide a discussion of how mode labels can be collected via a simple binary
460 “click” interface, either online (during demonstration collection) or offline (after collection). In
461 either case, we can label dense periods and exact waypoints using a single binary “click” variable
462 via an external button: to label a waypoint at the end of a sparse period, we provide a single click
463 at the waypoint state; to label a dense period, we sustain the click until the end of the dense period
464 (see left image in [Fig. 5](#)). Once clicks are labeled, we demarcate periods in between clicks as sparse
465 modes, and periods with sustained clicks as dense modes (see right image in [Fig. 5](#)).

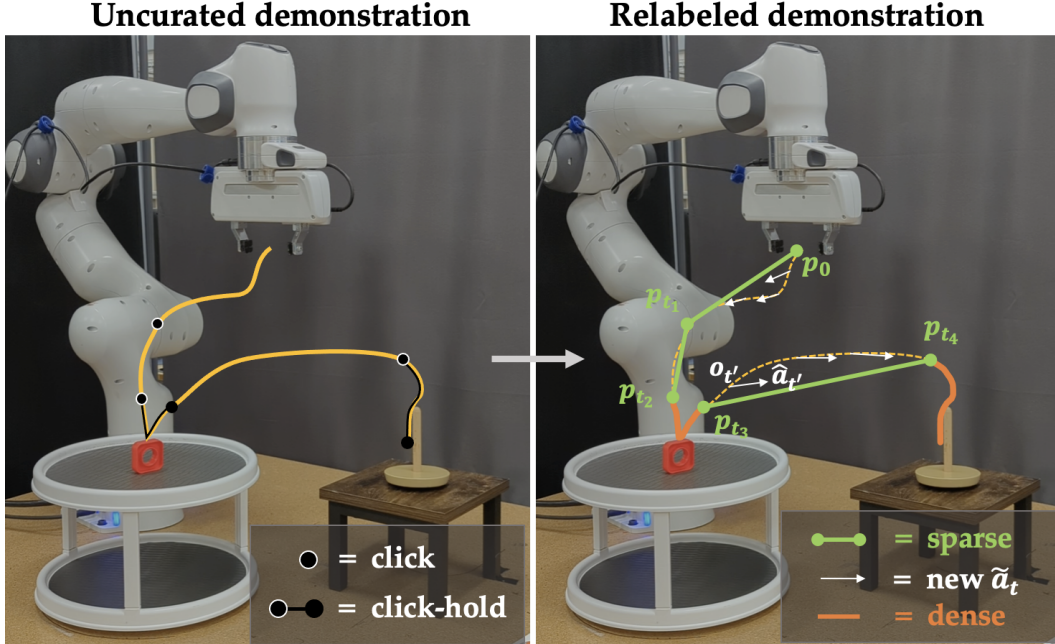


Figure 5: Mode labeling example for peg-insertion task. For each demo a human labels binary click signals at each time step (labeled online or offline) to segment trajectories into arbitrary sequences of sparse waypoint phases and dense action phases. **Left:** Uncurated demo, with single clicks and sustained clicks shown. **Right:** Relabeled demo, with waypoint and dense segments overlaid in green and orange, respectively. We also relabel actions for the states in sparse segments with the optimal waypoint reaching action shown in white. For sparse segments, the waypoint head of HYDRA is trained to output the final waypoint at each state along the trajectory.

466 With the trajectories segmented into sparse and dense modes, we can extract the desired future
 467 waypoint w_t for each o_t : if $m_t = 0$ (sparse), the future waypoint is the next labeled “single click”
 468 proprioceptive state $w_t = p_{t'}$ where $t' > t$ (for example, states o_t with $t_1 \leq t < t_2$ in Fig. 5 will use
 469 $w_t = p_{t_2}$). But if $m_t = 1$ (dense), the waypoint is the next proprioceptive state $w_t = p_{t+1}$. Thus we
 470 construct a dataset of \hat{D} of (o_t, a_t, w_t, m_t) tuples. Now the policy has full supervision to learn both
 471 the action and waypoint as well as the mode of operation. In Algorithm 1, we outline this process of
 472 turning a click-labeled dataset into per-step waypoints and mode labels.

Algorithm 1 Labeling Modes

```

1: Given click-labeled dataset:  $D = \{(o_t, a_t, c_t) \dots\}$ 
2:  $\hat{D} = \{\}$ 
3: for all  $t$  do
4:    $m_t = c_t \ \& \ (c_{t-1} \mid c_{t+1})$  ▷ Sustained click for dense
5:   // Mark single click as waypoint
6:    $\text{isolated} = \neg c_{t-1} \ \& \ c_t \ \& \ \neg c_{t+1}$ 
7:   // Mark start of dense period as waypoint
8:    $\text{start\_dense} = \neg c_{t-1} \ \& \ m_t$ 
9:   if  $\text{isolated}$  or  $\text{start\_dense}$  then
10:     $w_{t_p:t-1} = p_t$  ▷ Set previous waypoints
11:     $t_p = t$  ▷ start of next sparse phase
12:   else if  $m_t = 1$  then
13:     // During dense mode the next state is a waypoint
14:      $w_t = p_{t+1}$ 
15:      $t_p = t$ 
16:   Add  $(o_t, a_t, w_t, m_t)$  to  $\hat{D}$ 

```

473 B.2 Waypoint Controller

474 For all experiments in the main text, we use a linear controller T_{linear} for reaching waypoints online.
475 This means that when HYDRA predicts a waypoint period ($\tilde{m}_t = 0$), it will servo closed loop until
476 it reaches the predicted \tilde{w}_t or times out after N seconds. In all of our experiments, the waypoint
477 follower times out after $N = 5$ seconds if it has not reached the waypoint.

478 For this closed loop servoing during test time, the policy will still be *called*, but its outputs will
479 be ignored. This is important for recurrent models specifically (e.g., Dense Net), since the hidden
480 state for the policy should be updated similarly to how it was trained (on all states, even during
481 the sparse period). While this mitigates the changes in the hidden state, this might still induce a
482 different hidden state than was produced offline, since the human policy followed a non-optimal
483 path to reach waypoint w from state s_t , as compared to the optimal online trajectory generated by
484 T . For example, if the demonstrator follows an arc-like trajectory to pick up a coffee pod and marks
485 the waypoint right before picking up the coffee pod, then online the policy with T_{linear} will servo
486 to that waypoint directly; the hidden state for these two paths will likely be different. This problem
487 is difficult to observe in practice, and did not empirically show up in practice (as evidenced by the
488 improved performance of our method compared to baselines).

489 In theory, one could bypass this issue by “skipping” the hidden state of the policy over entire sparse
490 segments during training. Then during test time, if the policy outputs $\tilde{m}_t = 0$, the policy would not
491 be called again until reaching the output w_t . However, this requires loading entire sparse segments
492 and more in the training batches, which is computationally expensive and less simple than loading
493 batches of fixed horizon as is commonly done. We leave a broader analysis of the hidden state
494 problem for future work.

495 Additionally, we experimented with several controller gains and did not notice any effect on perfor-
496 mance. Therefore we choose a fast controller to reach waypoints. These gains are constant for all
497 experiments.

498 B.3 Mode Labeling Sensitivity

499 In our experiments, we noticed that mode labeling was quite robust to different labeling strategies
500 provided that the labeling strategy satisfies the following guidelines.

501 **Waypoint Following Behaviors:** Waypoint following behaviors should be labeled for free-space
502 motions in the environment, when the robot is “in transit” (e.g., reaching). As described in [Sec-](#)
503 [tion 4.1](#), a key consideration for mode labeling is making sure labels for sparse periods are compat-
504 ible with the waypoint controller T . For example, if we are following a linear controller, waypoint
505 segments should be reproducible with straight line segments from any start state along the waypoint
506 segment. For a given (m_t, w_t, s_t) , then if $m_t = 0$, we should be able to reach waypoint w_t from s_t
507 with T (i.e. without timing out). As mentioned in the main text, if T includes collision avoidance as
508 part of the controller, then we no longer have any requirements on waypoint following behaviors.

509 **Dense Object Interaction:** Dense periods should include (but is not limited to) all object interac-
510 tions in the scene where “collision” with the scene is necessary (e.g., grasping a coffee pod, inserting
511 the coffee pod into the coffee machine, picking up toast with a spatula). Humans excel at identify-
512 ing these types of interactions, so these segments are quite easy to label. The exact amount of time
513 “padded” onto these dense periods did not seem to affect learning in our experiments. Note that if
514 each entire demo is treated as a dense period, our algorithm reduces to BC.

515 **Labeling Strategy Consistency:** The final consideration is for the consistency of the mode labeling
516 strategy *between* different demonstrations. Variation in the exact boundaries / choices for waypoints
517 and dense segments is inevitable with human labeling. While the effects of certain types of variation
518 can be quite difficult to quantify in general, we believe that is important to minimize this variation
519 without adding additional burden on the user. In our experiments, for each task and dataset, we
520 have only one user provide the mode labels, according to a single strategy. For example, in the
521 *NutAssemblySquare* task, where the goal is to insert a square nut onto a peg, a user might define the
522 following strategy:

- 523 1. Reach waypoint above the square nut (sparse)
- 524 2. Go down, grasp, pick up (dense)
- 525 3. Move the nut up (sparse)
- 526 4. Move the nut above the insertion point (sparse)
- 527 5. precisely insert the nut on the peg (dense)

528 In general our method is quite robust to variations within a single mode labeling strategy (for a
 529 single labeler), and we do no additional post-processing on mode labels or waypoints in any of our
 530 experiments.

531 B.4 Training on Mode Labels

532 With labeled modes and waypoints, HYDRA learns to predict the mode, the waypoint, and the low-
 533 level action at every time step according to the loss in Eqn. 4. However, due to training a higher
 534 dimensional action space (e.g. for robot poses: $|\mathcal{A}| = 7 + 7 + 1$) with a supervised objective, over-
 535 fitting can be a key concern during training. For all vision-based experiments, we perform random
 536 cropping to 90% the image size. However, there are several interesting mode-specific augmentations
 537 that can be done using mode labels and waypoints to mitigate this problem:

538 **Mode Smoothing:** While the simple binary cross entropy mode loss in Eqn. 3 suffices for learning
 539 to predict modes, sometimes the hard boundary between segments can lead to mode oscillation or
 540 cycling when evaluating at test time. For example, model might predict a dense mode, then predict
 541 a sparse mode at the next step that brings it back to the previous state, and repeat. In these cases
 542 (which are rare in practice) it can be beneficial to *smooth* the mode labels to extract continuous
 543 probabilities for the mode label at each step: $p(\tau_m) = \text{convolve}(\tau_m, [\frac{1}{n}, \dots, \frac{1}{n}])$, where n is the kernel
 544 size. This yields the following loss:

$$\mathcal{L}_m(\theta) = -\mathbb{E}_{(o,a,w,m) \in \mathcal{D}} \left[p(m) \log \pi_{\theta}^M(m = 1|o) + (1 - p(m)) \log \pi_{\theta}^M(m = 0|o) \right] \quad (5)$$

545 With this smoothing of the mode labels, we are effectively removing the hard boundary between
 546 sparse and dense periods, which can help generalization for the mode prediction head of HYDRA
 547 at test time.

548 **Waypoint Period Augmentation:** It is common in the literature to add small amounts of proprio-
 549 ceptive state noise (increasing state diversity) to demonstrations. However, during object interaction
 550 (i.e. dense periods), this noise can make policy learning more difficult since minor variations in
 551 the state can have large changes in the action space. However, with knowledge of sparse and dense
 552 modes in HYDRA, we could add diverse state augmentations to the proprioceptive state during only
 553 the sparse periods. This waypoint period augmentation can help reduce overfitting in SparseNet,
 554 since we will learn to reach the same waypoint (action) from many different robot poses (state).

555 Both mode smoothing and waypoint augmentation, while not utilized in our experiments, illustrate
 556 the potential for new augmentation strategies that arise with access to mode labels.

557 C Model Architectures & Training

558 To train HYDRA, we use a similar procedure as in prior work [19, 14]. For each input of shape
 559 $D_1 \times \dots \times D_N$, we load sequential batches of size $B \times H \times D_1 \times \dots \times D_N$, where H is the horizon length.
 560 Next we outline the network design for HYDRA, and hyperparameters used in each environment.

561 C.1 Network Design

562 As described in Section 4, HYDRA consists of SparseNet, which predicts the waypoint trajectory
 563 τ_w , and DenseNet, which predicts the mode trajectory τ_m and low level action trajectory τ_a . Both
 564 networks condition on the same input observation space (proprioceptive state trajectory τ_{sp} and
 565 environment state τ_{se}). For vision based experiments, s^p consists of both wrist mounted and external
 566 camera observations. Each image is encoded via a ResNet18 architecture encoder (two encoders,
 567 E_{θ}^{ext} , $E_{\theta}^{\text{wrist}}$, with separate parameters) which is trained end-to-end. Next, the image encodings are
 568 concatenated along with the proprioceptive trajectory τ_{sp} .

Environment	Method	# Demos	B	H	lr	γ	β_m	$ i $	$ D $	$ S $	$ \pi_\theta^A $	$ \pi_\theta^M $	GMM
<i>NutAssemblySquare</i>	BC	200	256	-	1e-4	-	-	-	400	-	-	-	0
	BC-RNN	200	256	10	1e-4	-	-	-	400	-	-	-	0
	HYDRA	200	256	10	1e-4	0.5	0.01	-	400	200	200	200	0
<i>ToolHang</i>	BC	200	256	-	1e-4	-	-	-	400	-	-	-	5
	BC-RNN	200	256	10	1e-4	-	-	-	1000	-	-	-	5
	HYDRA	200	256	20	1e-4	0.5	0.1	-	1000	400	400	400	0
<i>KitchenEnv</i>	BC-RNN	100	16	10	1e-4	-	-	64	1000	-	-	-	5
	HYDRA	100	16	10	1e-4	0.5	0.01	64	1000	400	400	400	5
<i>PegInsertion</i>	BC-RNN	75	8	10	1e-4	-	-	64	1000	-	-	-	0
	HYDRA	75	8	10	1e-4	0.5	0.01	64	1000	1000	1000	1000	0
<i>MakeCoffee</i>	BC-RNN	100	8	10	1e-4	-	-	64	1000	-	-	-	0
	HYDRA	100	8	10	1e-4	0.5	0.01	64	1000	1000	1000	1000	0
<i>MakeToast</i>	BC-RNN	80	8	10	1e-4	-	-	64	1000	-	-	-	0
	HYDRA	80	8	10	1e-4	0.5	0.01	64	1000	1000	1000	1000	0

Table 1: Hyperparameters for each environment, from left to right: B is batch size, H is the horizon length for training, lr is the learning rate, γ is the per time step weighting of the current mode, β_m is the weighting of the mode loss, $|i|$ is the image encoding size (for each image), $|D|$ is the hidden-size for recurrent dense networks (DenseNet, BC-RNN) or the MLP width (BC), $|S|$ is the width of the SparseNet MLP (3 layers), $|\pi_\theta^A|$ is the width of the action head (2 layers), $|\pi_\theta^M|$ is the width of the mode head (2 layers), and finally GMM is the number of Gaussian mixtures (or 0 if deterministic) used for the dense action space. The top 3 rows are sim environments, where the first two are state only. The bottom three rows are vision-based real-world experiments. Hyperparameters stay mostly constant for HYDRA between experiments, with larger policy sizes for harder tasks. In almost all cases, BC-RNN, BC, and HYDRA share the same hyperparameters.

Algorithm 2 Training HYDRA

- 1: Given N (number of training steps)
 - 2: Given mode-labeled dataset: $\hat{D} = \{(\tau_o, \tau_a, \tau_w, \tau_m) \dots\}$
 - 3: Networks $E_\theta^{\text{ext}}, E_\theta^{\text{wrist}}, \pi_\theta^W, \pi_\theta^A, \pi_\theta^M$
 - 4: **for** i **in** range(N) **do**
 - 5: $\tau_o, \tau_a, \tau_w, \tau_m \sim \hat{D}$ ▷ Load ($B \times H \times \dots$)
 - 6: $\tau_i = E_\theta^{\text{wrist}}(\tau_o) \oplus E_\theta^{\text{ext}}(\tau_o) \oplus \tau_{sp}$ ▷ Encode
 - 7: $\tau_w = \pi_\theta^W(\tau_i)$ ▷ waypoint (SparseNet)
 - 8: $\tau_m = \pi_\theta^M(\tau_e)$ ▷ mode (DenseNet)
 - 9: $\tau_a = \pi_\theta^A(\tau_e)$ ▷ action (DenseNet)
 - 10: Compute $\mathcal{L}(\theta)$ in Eqn. 4 and update θ
-

569 C.2 Model & Training Details

570 Visual encoders use a ResNet-18 architecture trained end-to-end on both external images and end-
571 effector images. We train all methods for 500k training steps over 3 random seeds, and like prior
572 work we report the average over the best performing checkpoints per run [19]. We found that BC
573 policy performance fluctuates significantly even for neighboring checkpoints. However, unlike prior
574 work we use a *fixed* evaluation set of 50 episodes in simulation to choose the best checkpoint. This
575 reduces the likelihood of choosing the checkpoint that was evaluated on favorable environments
576 (i.e., rejection sampling of harder environment initialization).

577 For all experiments, our method uses an RNN (LSTM) for Dense Net (predicting the mode and the
578 dense action), and uses a separate MLP with the same inputs for the Sparse Net (predicting sparse
579 waypoints), as shown in Fig. 1.

580 The input embedding is then passed into SparseNet (MLP) which outputs the waypoint as a robot
581 pose (position and quaternion). DenseNet can be any sequential model (RNN, Transformer, etc) that
582 produces some temporal embedding τ_e (RNN in our case). This architecture is shown in Fig. 6, and
583 the training cycle is shown in Algorithm 2.

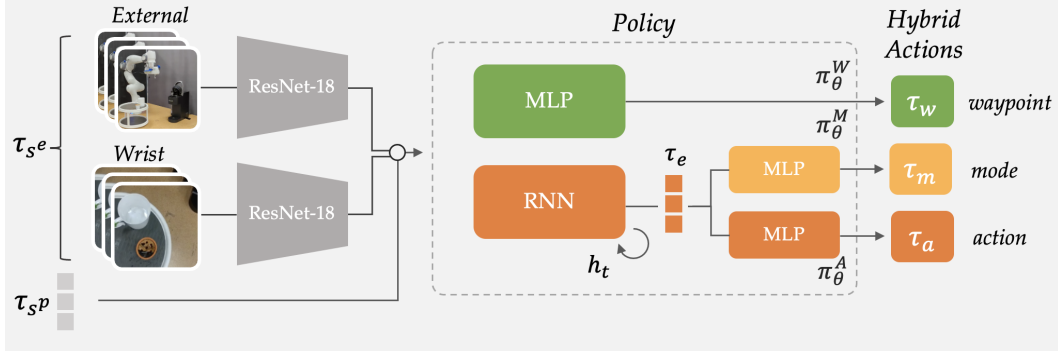


Figure 6: Specific instantiation of HYDRA for vision based experiments.

584 C.3 Evaluation Details

585 During evaluation (see Algorithm 3), the policy chooses the mode using \tilde{m}_t . If $\tilde{m}_t = 0$, the
 586 model will servo in a closed-loop fashion to the predicted waypoint \tilde{w}_t (Line 7) using controller
 587 T (Line 10). The policy is queried at every step to continually update the policy hidden state, but
 588 importantly its outputs are ignored until we reach the waypoint to avoid action prediction errors.
 (Line 4). If $\tilde{m}_t = 1$, the model will execute one step using the predicted dense action \tilde{a}_t (Line 14).

Algorithm 3 Test Time Execution

```

1: Given env,  $\pi(m, a, w|o)$ , initial state  $o_0$ , controller T
2:  $t = 0, w = \text{None}$ 
3: while not done do
4:    $\tilde{m}_t, \tilde{a}_t, \tilde{w}_t \sim \pi(\cdot|o_t)$  ▷ Sample policy
5:   // Check for new sparse mode
6:   if  $w$  is not set and  $\tilde{m}_t = 0$  then
7:      $w = \tilde{w}_t$  ▷ Set a new waypoint
8:   // Compute the waypoint-optimal action (sparse)
9:   if  $w$  is set but not reached and not timed-out then
10:     $\tilde{a}_t \leftarrow T(o_t, w)$  ▷ Compute waypoint-optimal action
11:   else
12:      $w = \text{None}$  ▷ Unset waypoint if reached
13:   // Step the environment
14:    $o_{t+1} = \text{env.step}(\tilde{a}_t)$ 
15:    $t = t + 1$ 

```

589

590 C.4 HYDRA Hyperparameters

591 The hyperparameters used in the main text for all six environments are shown in Table 1, for BC,
 592 BC-RNN, and HYDRA. Hyperparameters stay mostly constant for HYDRA across all of the ex-
 593 periments, with larger policy sizes for harder tasks. Additionally, in almost all cases, BC-RNN,
 594 BC, and HYDRA share the same hyperparameters where possible. In the real world experiments,
 595 hyperparameters are exactly the same both across methods and across environments.

596 D Additional Results & Analysis

597 In this section we show rollouts of our method and baselines, and then perform ablations of our
 598 method and analyze the results, including mode labeling sensitivity, mode label learning from less
 599 data, choices in action space design, different loss weightings, and robustness experiments. All
 600 ablations are performed on the *NutAssemblySquare* task unless otherwise stated.

601 D.1 Rollouts for Real Environments

602 Fig. 7 shows example rollouts from the uncurated demonstration, the learned BC-RNN policy, and
 603 HYDRA. Qualitatively, in the top row of Fig. 7 we see that HYDRA produces more consistent and

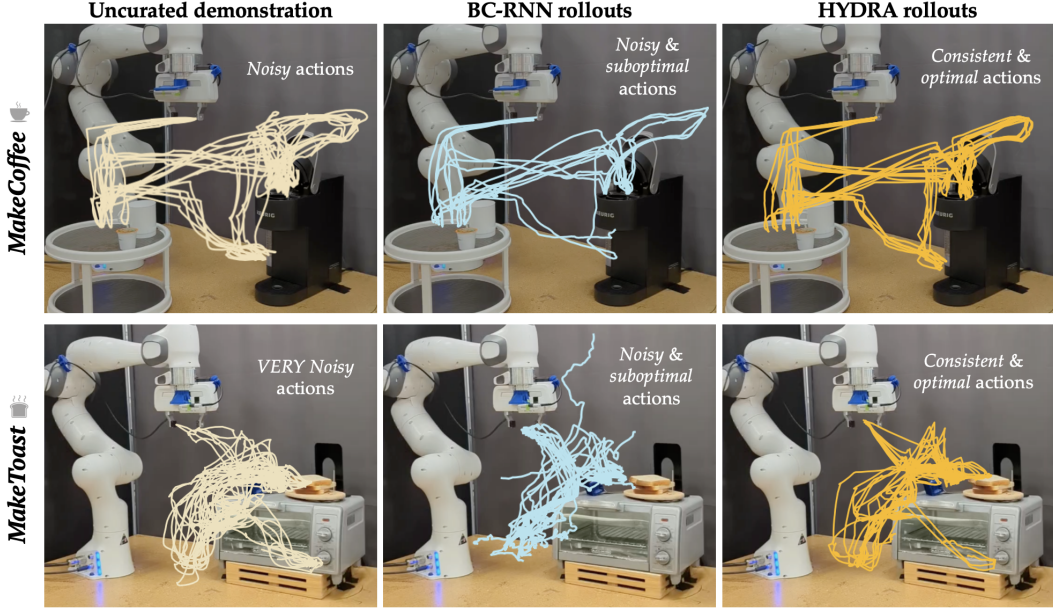


Figure 7: *MakeCoffee* (top) and *MakeToast* (bottom) rollouts, with the demos (left), HYDRA rollouts (middle), and BC-RNN rollouts (right). Our method produces more consistent and optimal actions compared to both BC-RNN and the demonstrations, and thus is able to stay within the narrow success “band” of the state distribution. BC-RNN has many sub-optimal behaviors, leading to less completed trajectories in middle column. The demonstrations for *MakeToast* are even noisier than those in *MakeCoffee*, leading to even more noticeable distribution shift for BC-RNN in the *MakeToast* task. In contrast, HYDRA *curates* the demonstrations in *MakeToast* using sparse and dense periods to follow more consistent paths, thus leading to higher success.

604 optimal trajectories at evaluation time that help the policy to stay within the narrow “band” of the
 605 successful state distribution at test time, thus improving performance.

606 For the long horizon *MakeToast* task, the performance of HYDRA is much better than BC-RNN,
 607 but lower overall than in *MakeCoffee*. We hypothesize that the difference between this task and
 608 *MakeCoffee* is primarily in the consistency of demonstrated actions (see demonstration rollouts in
 609 Fig. 7), with significant variation in the behaviors for nearby states especially during dense periods.
 610 This leads to BC-RNN having highly noisy and sub-optimal actions, which manifest quite notice-
 611 ably in Fig. 7. However, HYDRA yields much more consistent and optimal motions, reducing the
 612 distribution-shift problem.

613 D.2 Mode Sensitivity

614 Next, we consider the sensitivity of HYDRA to mode labels, specifically in terms of the number of
 615 labeled waypoints in each episode. In Table 2, we ablate the number of waypoints by introducing N
 616 intermediate waypoints in every sparse segment, for $N = 1$ and $N = 2$. Since there are at least 3
 617 sparse segments labeled in each demo in *NutAssemblySquare*, this corresponds to adding at least 3 or
 618 6 more waypoints to each demonstration, respectively. We see that performance drops are relatively
 619 minor in both cases, showing that HYDRA is robust to different waypoint choices. We hypothesize
 620 that the reason for the minor performance change when adding more waypoints is that SparseNet
 must learn a more complex waypoint space that is more multi-modal.

Base	Add-1	Add-2
90.0	86	80.0

Table 2: Success rates for HYDRA when artificially more waypoints are added to sparse periods. Adding intermediate waypoints to sparse segments has only a minor effect on performance despite the increase in complexity of the pose action space.

621

622 **D.3 Learning Mode Labels from Less Data**

623 Providing mode labels can be an additional overhead when training HYDRA. To reduce overhead,
 624 we might want to learn the mode labels from a few labeled examples, and use this to relabel the rest
 625 of the dataset. To show the promise of such an approach, we learn to predict the “click state” at
 626 each time step (same as in Fig. 5) using a simple RNN architecture with the same parameters as the
 627 model used for training. This model outputs two logits, one for the mode itself (m_t), and one that
 628 represents a switching criteria between segments (s_t). This allows us to predict not only the sparse
 629 or dense label, but also the waypoint label for each sparse segment. We additionally smooth both
 630 m_t and s_t as is commonly done in binary sequence prediction tasks. In Table 3, we demonstrate that
 631 we can learn mode labels from 25% of the data with only a 10% drop in performance for the square
 task, and even less of a drop when training on 50% or 75% of the data.

90%	75%	50%	25%
92	88	86	82

Table 3: Success rates for HYDRA for *NutAssemblySquare* when the mode labels are learned (predicting “click state” in Fig. 5).

632
 633 With this preliminary evidence, we believe the sample efficiency of this mode learning procedure can
 634 be improved by incorporating prior data from a wide range of tasks, potentially even using labeled
 635 internet data. To address the multi-modality of mode labels that might occur when having multiple
 636 people provide labels, future work might leverage few-shot or in-context learning approaches to
 637 adapt to a particular *style* of mode labeling.

638 **D.4 Variations in the Action Space**

639 Why do we need the dense period at all? In Table 4, we compare HYDRA’s hybrid action space
 640 to waypoint only ablations, both with and without the test-time controller T_{linear} . With T_{linear} , the
 641 model outputs a waypoint and the robot reaches that waypoint using T_{linear} without querying the
 642 policy (“open loop”), and without T_{linear} , the model outputs a new waypoint every step which gets
 643 converted to action a using T_{linear} (“close loop”).

644 First we show results for WP-Next{N} in Table 4, where waypoints are the pose of the robot N steps
 645 in the future at each state (hindsight relabeling). Second, we compare to WP-Mode, which uses
 646 the same mode labels in HYDRA to get more intelligent future waypoints during sparse segments.
 647 No pose-based models see any success, which we hypothesize is due to the mismatch between
 648 the human action a and the online action $T_{\text{linear}}(o, w)$, which can lead to out of distribution states.
 649 Even in the open loop case, the waypoint only models are unable to perform the task, with failures
 650 involving imprecise behaviors during dense periods where exact velocities truly matter.

651 We additionally compare our method with and without the use of T_{linear} online (first column in
 652 Table 4). We see that HYDRA greatly benefits from the online waypoint controller, since T_{linear}
 653 follows an optimal path while the policy-in-the-loop approach leaves room for compounding errors
 654 in both the mode, action, and waypoint prediction. This once again illustrates that HYDRA yields
 more consistent and optimal actions by employing a hybrid action abstraction.

	Ours	WP-Next1	WP-Next2	WP-Next5	WP-Mode
w/ T	90.0	0.0	0.0	2.0	0.0
w/o T	58.0	0.0	0.0	0.0	0.0

Table 4: Success rates for different action spaces. HYDRA uses a hybrid action space, while the the rest use a pose-based action space. Top row: waypoints are reached using T_{linear} before calling the policy again (“open” loop). Bottom row: waypoint actions are computed at every step and instead of reaching the action, the policy will convert a waypoint w to dense action a using T_{linear} (“closed” loop). WP-Next{N} uses the proprioceptive state N steps in the future as the waypoint for each state. WP-Mode uses the same mode labels as in HYDRA to get the waypoints, but does not implement a hybrid action space. None of the pose-based action spaces get reasonable performance, showing the importance of both dense actions and waypoint phases.

655
 656 **D.5 Ablating Mode Weighting (γ)**

657 We also show the effect of different values of γ , the weight of the current mode loss. If for a given
 658 step in training mode $m_t = 0$ (sparse), then we weight the sparse waypoint loss for w_t with $1 - \gamma$ and

659 the dense action loss for a_t with γ . Lower γ thus corresponds to fitting the current mode action loss
 660 more than the other mode’s loss. Therefore, γ also controls the contribution of the relabeled actions
 661 during sparse periods to the overall objective in Eq. (2). We use $\gamma = 0.5$ in most experiments,
 662 meaning both action (waypoint and dense action) losses are weighted equally during training. We
 663 provide a sweep over γ in Table 5 for *NutAssemblySquare* and *ToolHang*, and we see that choosing
 664 γ only has a minor effect. Nonetheless, $\gamma = 0.5$ is consistently the best. This illustrates that (1)
 665 HYDRA is fairly robust to γ , (2) learning relabeled dense actions during sparse periods and sparse
 666 actions during dense periods is beneficial to performance – this supports the claim in Section 4.1
 667 that training on relabeled dense actions outperforms uncurated dense actions and

	$\gamma = 0.1$	$\gamma = 0.2$	$\gamma = 0.4$	$\gamma = 0.5$
Square	80.0	84.0	88.0	90.0
ToolHang	60.0	62.0	58.0	64.0

Table 5: Success rates for different values of γ for both *NutAssemblySquare* and *ToolHang*. For both *NutAssemblySquare* and *ToolHang*, γ does not have a large effect. We saw even less of a change for vision based experiments. Thus for real world experiments, we fix $\gamma = 0.5$ (no mode-specific weighting).

668 D.6 Transformer-based architecture

669 In Table 6 we show the performance of a purely transformer-based BC implementation on the *KitchenEnv*
 670 task. We see in this long horizon task that BC-RNN notably outperforms BC-Transformer in
 671 this single-task imitation learning setting, and we found similar drops in performance for the state-
 672 based simulation experiments. Thus, we did not include BC-Transformer as a baseline in our real
 673 world experiments. We note that VIOLA, which uses a similar underlying transformer but with a
 674 object-centric input representation, performs notably better on *KitchenEnv* than BC-Transformer.

	BC-RNN	BC-Transformer	VIOLA	HYDRA
Square	84	78.0	–	90.0
Kitchen	52.0	24.0	78.0	87.0

Table 6: Success rates for different values of BC architectures on *NutAssemblySquare* (state-based) and *KitchenEnv* (vision-based). For *NutAssemblySquare*, we see that using BC-Transformer minorly reduces performance. In *KitchenEnv*, we see a larger performance drop for BC-Transformer compared to BC-RNN. VIOLA proves a superior transformer based architecture compared to simple BC-Transformer for *KitchenEnv*. In all cases, HYDRA beats both RNN and Transformer-based baselines. All models share the same visual encoder structure and action spaces as described in Table 1.

675 D.7 Robustness of HYDRA to system noise

676 In Section 3 we noted the fundamental trade-off between consistent actions and state diversity. HY-
 677 DRA breaks this tradeoff by relabeling actions in offline data, encouraging action consistency with-
 678 out reducing the state coverage of the data. To show that HYDRA still benefits from the state
 679 diversity in human data, in Table 7 we analyze the effect of system noise on HYDRA and BC. We
 680 find that HYDRA only drops from 90% to 86% (4% drop) under the same system noise as used
 681 with BC. This shows that not only does HYDRA capture the state diversity in human data, but it is
 682 able to be even more robust to distribution shift than BC. We attribute this boost in part to the use
 683 of a closed loop waypoint controller, which consistently reaches the waypoint under system noise.
 684 This also supports the claim made in Section 6 that the gap in performance between HYDRA and
 685 baselines in real compared to simulation experiments can in part be attributed to the added system
 686 noise found in the real world.

	Base	Noise=0.1	Noise=0.3
BC-RNN	84	76.0	60.0
HYDRA	90	92.0	86.0

Table 7: The effect of increasing system noise (columns left to right) on BC-RNN (top row) and HYDRA (bottom row) trained on human data for *NutAssemblySquare*. While BC-RNN drops 24% under the max system noise, HYDRA only drops 4%, illustrating the ability of HYDRA to capture state diversity and thus be robust to distribution shift.